

# Serendipitous Discovery of Short Peptides from Natural Products as Tyrosinase Inhibitors

Nai-Wan Hsiao,<sup>†</sup> Tien-Sheng Tseng,<sup>‡</sup> Yu-Ching Lee,<sup>§,V,¶</sup> Wang-Chuan Chen,<sup>⊥,#</sup> Hui-Hsiung Lin,<sup>‡</sup> Yun-Ru Chen,<sup>†,◆</sup> Yeng-Tseng Wang,<sup>||</sup> Hung-Ju Hsu,<sup>‡</sup> and Keng-Chang Tsai\*,<sup>‡</sup>

<sup>†</sup>Institute of Biotechnology, National Changhua University of Education, Changhua 500, Taiwan

<sup>‡</sup>National Research Institute of Chinese Medicine, Ministry of Health and Welfare, Taipei 112, Taiwan

<sup>§</sup>The Institute for Cancer Biology and Drug Discovery, College of Medical Science and Technology, Taipei Medical University, Taipei 110, Taiwan

<sup>V</sup>Antibody and Hybridoma Core Facility, Taipei Medical University, Taipei 110, Taiwan

<sup>¶</sup>The Center of Translational Medicine, Taipei Medical University, Taipei 110, Taiwan

<sup>⊥</sup>The School of Chinese Medicine for Post-Baccalaureate, I-Shou University, Kaohsiung, Taiwan

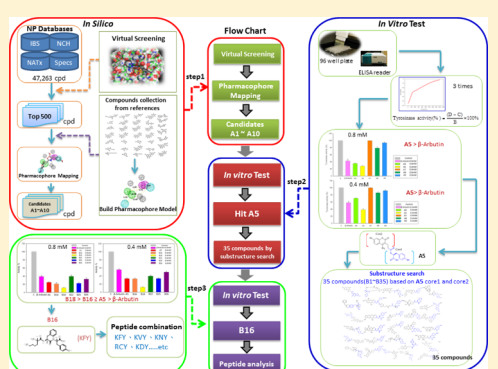
<sup>#</sup>Department of Chinese Medicine, E-Da Hospital, Kaohsiung, Taiwan

<sup>◆</sup>Institute of Bioinformatics and Structural Biology, National Tsing Hua University, Hsinchu 30013, Taiwan

<sup>||</sup>Department of Biochemistry, College of Medicine, Kaohsiung Medical University, Kaohsiung, Taiwan

## Supporting Information

**ABSTRACT:** Tyrosinase, which is the crucial copper-containing enzyme involved in melanin synthesis, is strongly associated with hyperpigmentation disorders, cancer, and neurodegenerative disease; thus, it has attracted considerable interest in the fields of medicine and cosmetics. The known tyrosinase inhibitors show numerous adverse side effects, and there is a lack of safety regulations governing their use. As a result, there is a need to develop novel inhibitors with no toxicity and long-term stability. In this study, we use molecular docking and pharmacophore modeling to construct a reasonable and reliable pharmacophore model, called Hypo 1, that could be used for identifying potent natural products with crucial complementary functional groups for mushroom tyrosinase inhibition. It was observed that, out of 47 263 natural compounds, **A5** structurally resembles a dipeptide (WY) and natural compound **B16** is the equivalent of a tripeptide (KFY), revealing that the C-terminus tyrosine residues play a key role in tyrosinase inhibition. Tripeptides RCY and CRY, which show high tyrosinase inhibitory potency, revealed a positional and functional preference for the cysteine residue at the N-terminus of the tripeptides, essentially determining the capacity of tyrosinase inhibition. CRY and RCY used the thiol group of cysteine residues to coordinate with the Cu ions in the active site of tyrosinase and showed reduced tyrosinase activity. We discovered the novel tripeptide CRY that shows the most striking inhibitory potency against mushroom tyrosinase ( $IC_{50} = 6.16 \mu M$ ); this tripeptide is more potent than the known oligopeptides and comparable with kojic acid-tripeptides. Our study provides an insight into the structural and functional roles of key amino acids of tripeptides derived from the natural compound **B16**, and the results are expected to be useful for the development of tyrosinase inhibitors.



## INTRODUCTION

Melanin is mainly produced by the melanocytes located in the basal layer of the epidermis.<sup>1,2</sup> The overproduction and accumulation of melanin results in hyperpigmentation, which darkens the skin and produces freckles and dark spots,<sup>3</sup> or even leads to melanoma.<sup>4</sup> Tyrosinase (EC 1.14.18.1), which is a multifunctional enzyme that contains two Cu atoms in its active site, is widely distributed in fungi, plants, and animals.<sup>5</sup> Tyrosinase plays a critical role in melanin biosynthesis—it catalyzes not only the hydroxylation of L-tyrosine to L-3-(3,4-dihydroxyphenyl)-alanine (L-DOPA) but also the subsequent oxidation of L-DOPA to dopaquinone.<sup>6,7</sup> The oxidation of L-

tyrosine to melanin is essential for the coloring of skin, eyes, and hair, as well as for food browning.<sup>8</sup> It has also been reported that tyrosinase contributes to hyperpigmentation disorders, cancer, and neurodegeneration associated with Parkinson's disease.<sup>4,9,10</sup> This makes tyrosinase an essential material for the design, screening, and development of potent inhibitors in the fields of medicine, cosmetics, and agriculture.<sup>5,11</sup>

**Received:** May 1, 2014



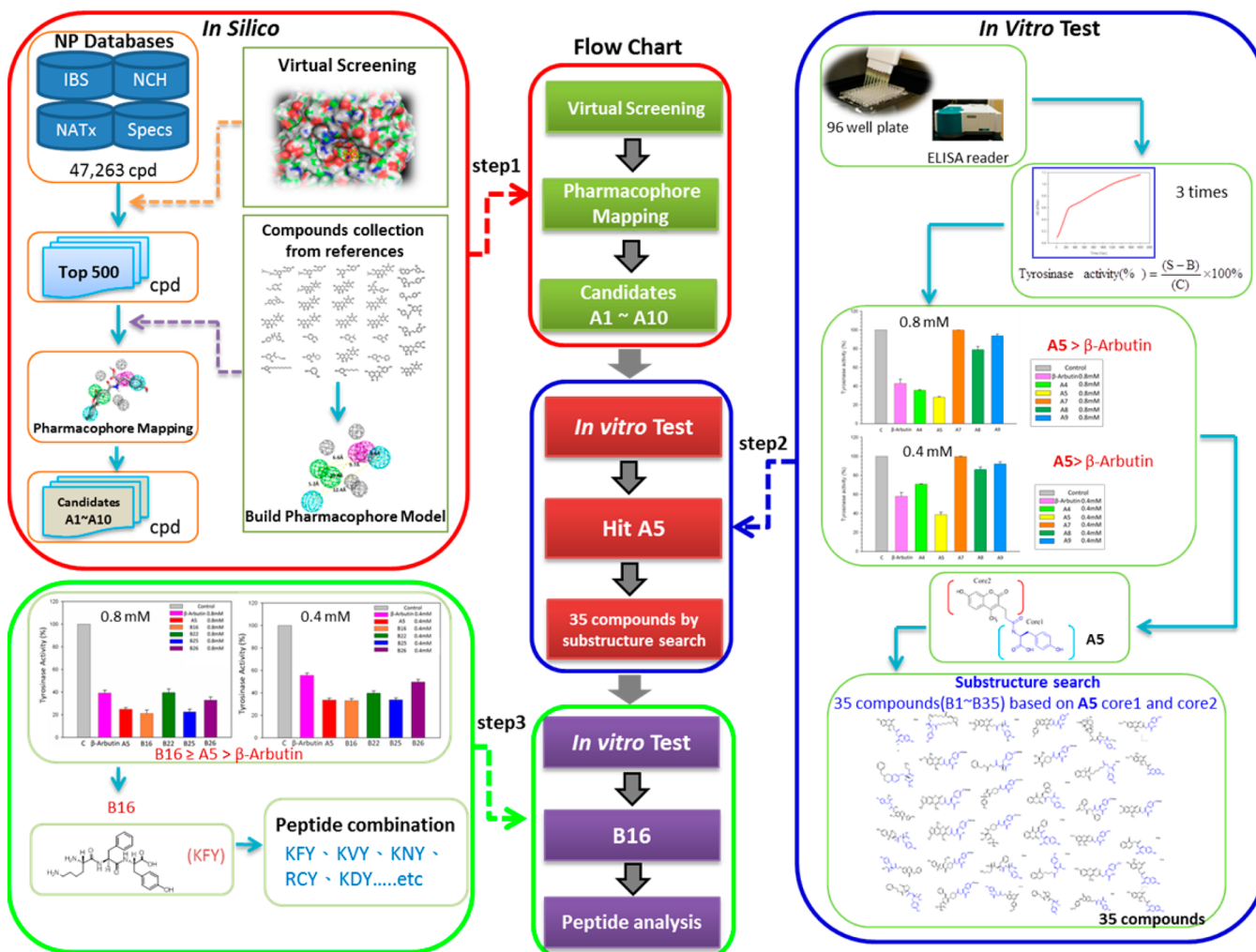


**Figure 1.** Flowchart of the combination of structure-based molecular docking and ligand-based pharmacophore modeling used to construct Hypo 1, which was used to identify potential natural products and crucial complementary functional groups for mushroom tyrosinase inhibition.

A large number of tyrosinase inhibitors have been reported, and their inhibitory activity against tyrosinase can be categorized according to the following functions: (1) reducing agents causing the chemical reduction of dopaquinone, (2) *o*-dopaquinone scavengers, (3) alternative enzyme substrates, (4) nonspecific enzyme inactivators, (5) specific tyrosinase inactivators, and (6) specific tyrosinase inhibitors.<sup>7</sup> However, only specific tyrosinase inactivators and inhibitors are regarded as "true inhibitors": they actually bind to the enzyme and inhibit its activity. For example, kojic acid and ellagic acid chelate with Cu ions at the catalytic sites of tyrosinase,<sup>7,12</sup> hydroquinone and arbutin compete at the active sites where tyrosine binds,<sup>5,13</sup> and both exhibit sufficiently potent inhibitory activity against tyrosinase. Although these inhibitors can effectively inhibit tyrosinase activity, their use is restricted, because of their adverse side effects and the lack of safety regulations governing their use.<sup>14</sup> Hydroquinone has been found to be a potential mutagen for mammals and can cause skin allergies. The product of hydroquinone oxidation, benzoquinone,<sup>15</sup> is a known mutagen; it can damage DNA,<sup>16</sup> and it is cytotoxic to hepatocytes and melanocytes<sup>17</sup> and may be carcinogenic.<sup>18</sup> Unfortunately, none of the alternatives to hydroquinone, such as kojic acid and arbutin,<sup>15</sup> offer a safe and effective replacement. In addition, the carcinogenicity of kojic

acid has spurred Japanese officials to ban its use in skin treatments.<sup>19</sup>

Unlike existing tyrosinase inhibitors, natural products show high potential for use in new drug development, because they are considered to be safe and free from adverse side effects. This advantage together with the determined crystal structure of mushroom tyrosinase (PDB ID: 2Y9X) makes it feasible to screen potent inhibitors from natural resources against tyrosinase by means of molecular docking and computer-aided drug design. In silico virtual screening can predict the biological activity of compounds from their structural properties, at considerably low cost and in a short time, quickening the pace of investigations of drugs with specific biological activity. For the accurate screening of potent tyrosinase inhibitors, the structural features responsible for interacting with the target site should be considered. Quantitative structure-activity relationship (QSAR) is a technique to estimate a compound's structural features required for the interaction of the compound with a receptor. To discover and design potent tyrosinase inhibitors, we have investigated and constructed a ligand-based pharmacophore model.

In this study, we employed structure-based molecular docking together with ligand-based pharmacophore modeling methods to construct a reasonable and reliable pharmacophore

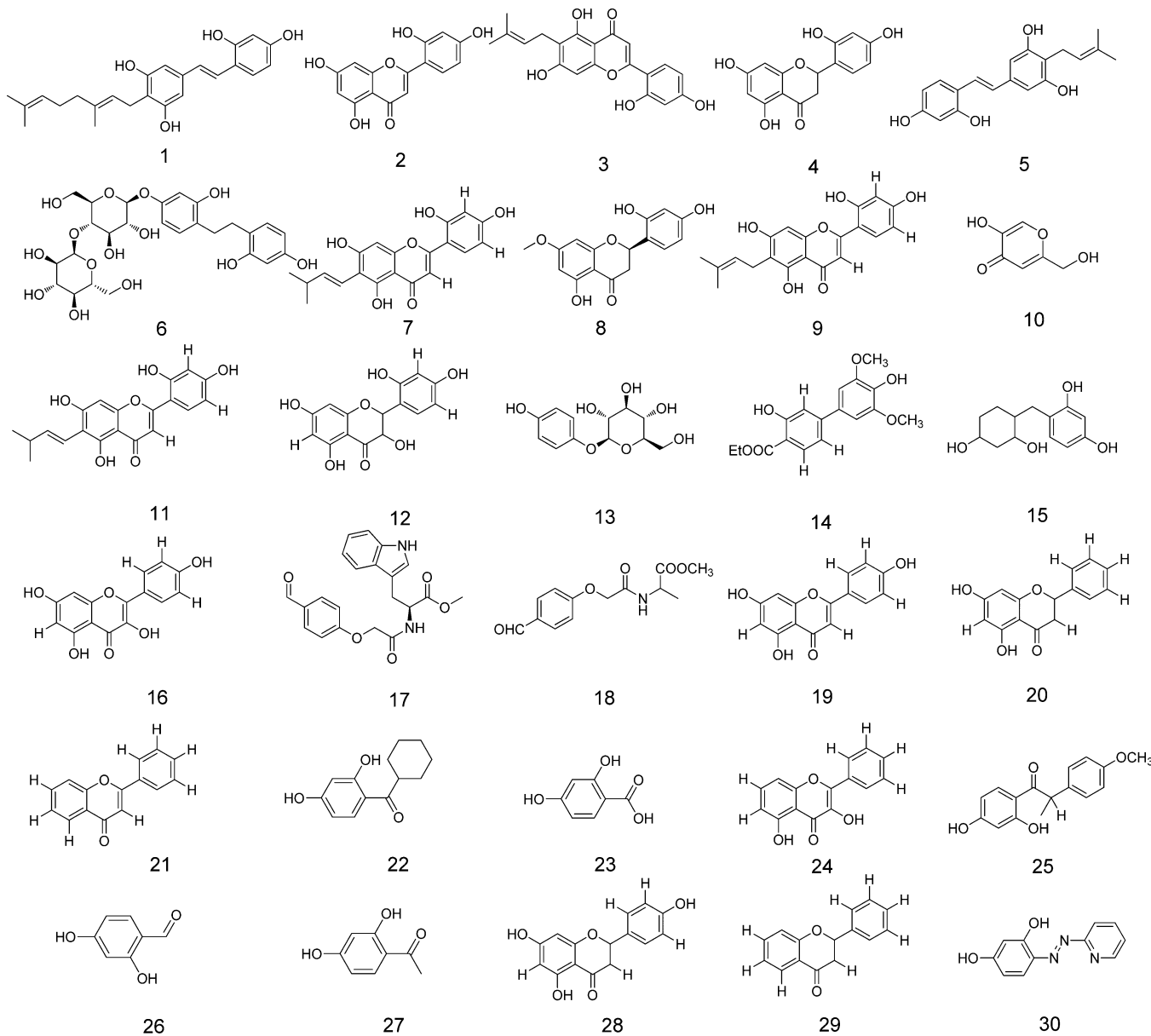


Figure 2. Chemical structures of all 30 training set molecules used for HypoGen pharmacophore generation.

model that can be used to identify the essential complementary functional groups that can act as mushroom tyrosinase inhibitors. We also used the pharmacophore model to screen natural compounds with potential tyrosinase inhibitory activity. Natural product **B16** (InterBioScreen (IBS) ID: STOCK1N-51005), with the chemical structure of KFY, was optimized to enhance its tyrosinase inhibitory potency. Tripeptides CRY and RCY, which show higher tyrosinase inhibitory activity, compared to arbutin and known peptide inhibitors,<sup>20–23</sup> were evaluated for their functional complementarities by using the pharmacophore model and investigated for their interactions with tyrosinase in order to elucidate the inhibitory mechanism. This study provided an insight into the structural and functional roles of key amino acids in tripeptides derived from natural compounds, and the results obtained are expected to be useful for the development of tyrosinase inhibitors.

## RESULTS

**In Silico Study.** *1. Multiple Sequence Alignment.* Sequence alignment is an important tool for identifying regions with similarities among proteins and establishing functional and structural relationships between different proteins. The crystal structure of human tyrosinase has not been elucidated to date. The multiple sequence alignment of representative tyrosinase proteins and human tyrosinase was evaluated in this study. We retrieved known homologous structures of human tyrosinase from the Protein Data Bank (PDB). The following representatives of tyrosinase proteins were chosen: *Agaricus bisporus* (mushroom) tyrosinase (PDB ID: 2Y9X) A chain, *Streptomyces castaneoglobisporus* tyrosinase (PDB ID: 1WX2) A chain, *Bacillus megaterium* tyrosinase (PDB ID: 3NM8) A chain, and the human tyrosinase sequence (see Figure S1 in the Supporting Information). Using the Discovery Studio 3.5 alignment protocol, each tyrosinase sequence was aligned. The sequence alignment represented 25 identical residues, and there were six highly conserved histidine residues among the

**Table 1.** Actual and Estimated IC<sub>50</sub> ( $\mu$ M) for the Training Set Based on the Best Pharmacophore Hypothesis Hypo 1

No.	name or code	estimated IC <sub>50</sub> ( $\mu$ M)	actual IC <sub>50</sub> ( $\mu$ M)	error	estimated scale <sup>a</sup>	actual scale <sup>a</sup>	ref
1	Chlorophorin	0.15	0.26	-1.7	+++	+++	24
2	Norartocarpentin	4	0.46	+8.5	+++	+++	25
3	Artocarpesin	0.44	0.52	-1.2	+++	+++	25
4	Steppogenin	4.5	0.57	+7.9	+++	+++	25
5	4-prenyloxyresveratrol	0.61	0.66	-1.1	+++	+++	24
6	Cpd5	1.6	0.68	+2.4	+++	+++	26
7	Oxyresveratrol	3.7	0.98	+3.8	+++	+++	24
8	Artocarpanone	3.6	1.5	+2.4	+++	+++	25
9	Cpd35	3.7	13	-3.6	+++	++	24
10	kojic acid	120	14	+8.5	++	++	24
11	isoartocarpesin	3.7	21	-5.7	+++	++	24
12	(+)-dihydromorin	4.4	25	-5.6	+++	++	24
13	Arbutin	11	40	-3.7	++	++	24
14	Cpd22	68	50	+1.4	++	++	27
15	Cpd34	110	58	+1.8	++	++	24
16	Keampferol	270	103	+2.6	+	+	24
17	Cpd6g	95	110	-1.2	++	+	28
18	Cpd6b	110	160	-1.5	+	+	28
19	Apigenin	260	185	+1.4	+	+	24
20	(-)-pinocembrin	140	200	-1.4	+	+	24
21	flavanone	170	200	-1.2	+	+	24
22	Cpd30	140	200	-1.4	+	+	24
23	Cpd28	150	200	-1.3	+	+	24
24	chrysin	130	200	-1.5	+	+	24
25	(-)-angolensin	110	200	-1.8	+	+	24
26	Cpd26	160	200	-1.3	+	+	24
27	Cpd27	150	200	-1.3	+	+	24
28	( $\pm$ )-naringenin	140	200	-1.4	+	+	24
29	( $\pm$ )-flavanone	150	200	-1.4	+	+	24
30	Cpd31	170	436	-2.6	+	+	24

<sup>a</sup>Activity scale: highly active (<5  $\mu$ M, +++), moderately active (5–100  $\mu$ M, ++), and inactive (>100  $\mu$ M, +). Detailed information on synthesis, separation, and biological data is reported in the literature.

tyrosinases. *A. bisporus* (mushroom) tyrosinase shares sequence identity (22%) with humans, *S. castaneoglobisporus*, and *B. megaterium* tyrosinase. We used *A. bisporus* (mushroom) tyrosinase as a target for *in silico* and *in vitro* screening, because it is the most commonly consumed species worldwide and has a similar homologous structure.

**2. Virtual High-Throughput Screening.** As the flowchart in Figure 1 shows, the *in silico* screening consisted of two steps in the present study, i.e., molecular docking (structure-based method) and pharmacophore modeling (ligand-based method). A total of 47 263 natural products were retrieved from natural product databases, including 37 224 compounds from the InterBioScreen (IBS, <http://www.ibscreen.com>) diversity set, 794 compounds from Specs (<http://www.specs.net>), and 9245 compounds from NCH and NATx (semisynthetic compounds, <http://www.ac-discovery.com/>). First, molecular docking analysis was conducted using Genetic Optimization for Ligand Docking (GOLD), to identify the bioactive molecules from the natural product databases. GOLD is an automated ligand docking program that uses a genetic algorithm (GA) to explore the full range of ligand conformational flexibility with partial flexibility of the protein, and it satisfies the basic requirement that the ligand must substitute loosely bound water upon binding. To prepare compounds for docking analysis, all the natural products were processed by using the following steps: (1) two-dimensional (2D) structures were converted into three-dimensional (3D) structures, (2) charges were calculated,

and (3) H atoms were added. To validate the accuracy of docking protocol, the co-crystallized mushroom tyrosinase inhibitor, Tropolone, was redocked into the active site of the mushroom tyrosinase (PDB ID: 2Y9X). A RMSD value between crystallized structure and docking pose of Tropolone is  $\sim$ 0.5 Å. We also used the same procedures as a validation to dock all the natural products. Subsequently, they were docked according to the X-ray crystal structure of mushroom tyrosinase (PDB ID: 2Y9X). After the molecular docking examination, the 500 top-ranked compounds were selected according to the structure of the mushroom tyrosinase binding site. A collection of known tyrosinase inhibitors from the literature was used to construct the hypothetical pharmacophore models (see the discussion of pharmacophore modeling below). After the construction of the best pharmacophore model, the top 500 compounds were screened against the pharmacophore model to identify potential compounds that possess the complementary functional groups from the correct spatial arrangement.

**3. Pharmacophore Model Generation.** In the current study, 30 representative, structurally diverse tyrosinase inhibitors, with concentrations covering 4 orders of magnitude (from 0.26  $\mu$ M to 346  $\mu$ M),<sup>24–28</sup> were used as the training set for developing the pharmacophore model (Figure 2 and Table 1). Another 20 tyrosinase inhibitors were used as the test set<sup>29–40</sup> (see Figure 3). Furthermore, the top 10 hypotheses were generated by using the 3D-QSAR Pharmacophore Generation module

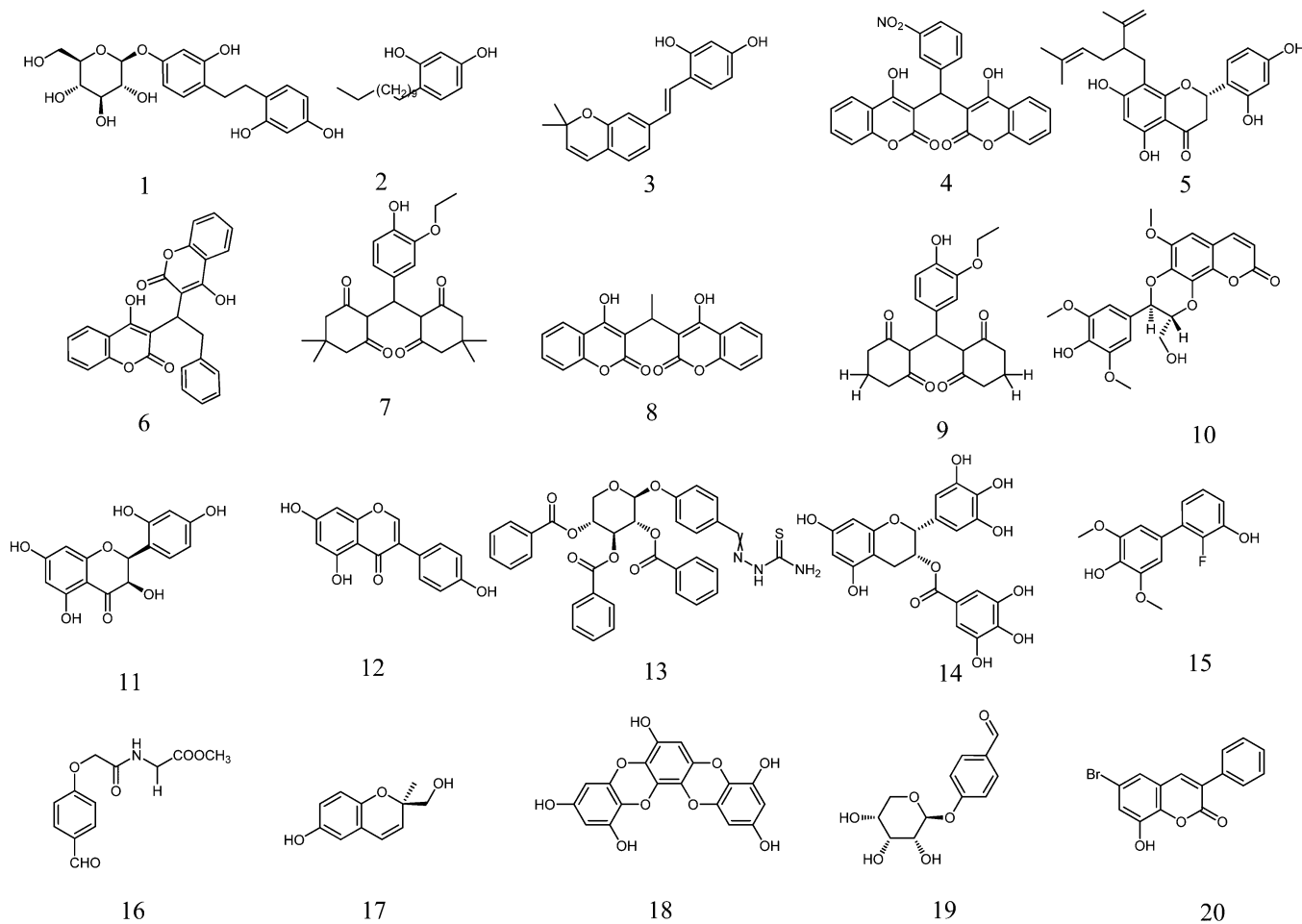


Figure 3. Chemical structures of all 20 test set molecules.

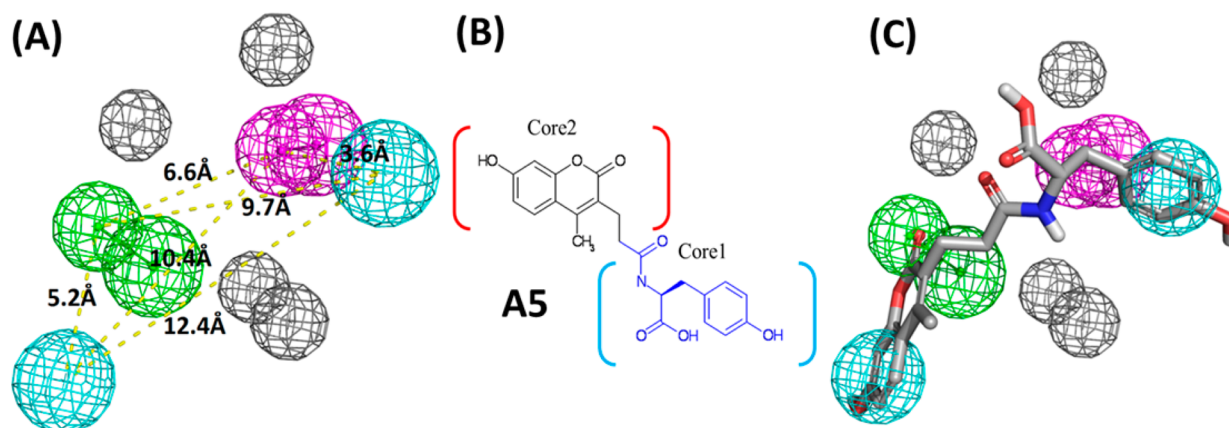
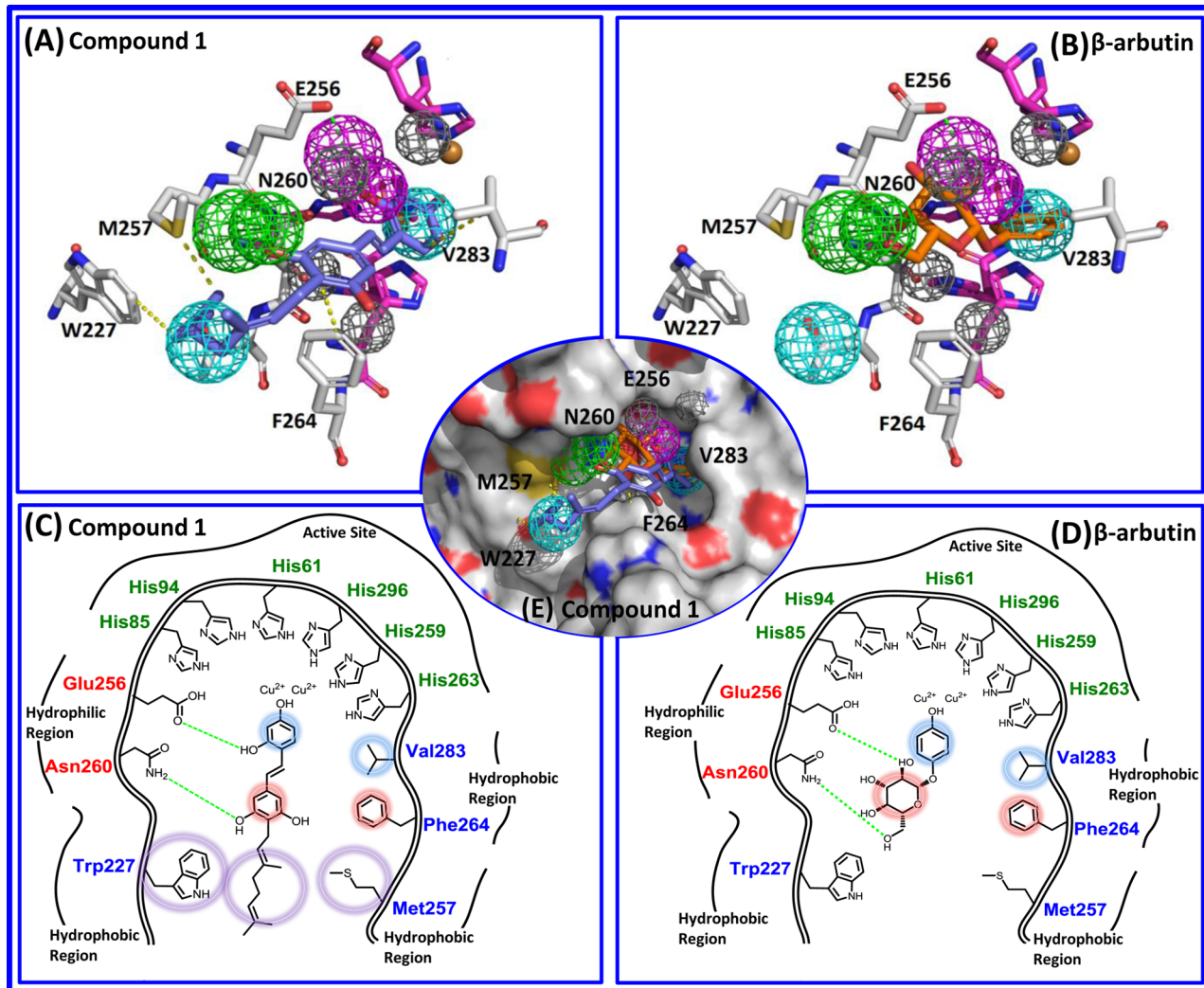


Figure 4. Schematic representation and structural information on Hypo 1 and the A5 molecule. (A) Features at a specific distance correspond to the best pharmacophore model Hypo 1. (Features are color-coded as follows: blue, hydrophobic; green, hydrogen-bond acceptor; magenta, hydrogen-bond donor; and dark gray, excluded volume.) (B) The chemical structure of the A5 molecule consists of two major moieties: Core1 and Core2. (C) Mapping of A5 (ball and stick) onto the Hypo1 hypothesis.

implemented in Discovery Studio 3.5, and they were ranked according to their “total cost” (see Table S2 in the Supporting Information). The top 10 hypotheses consisted of distinct combinations of a hydrogen-bond acceptor, a hydrogen-bond donor, two hydrophobic groups, and four excluded volumes. For the top 10 hypotheses, the parameters of statistical significance, such as the cost value, correlation coefficient ( $r$ ), and root mean square (RMS) deviations, and features, are listed

in Table S2 in the Supporting Information. The fixed cost of the 10 top-scoring hypotheses was 98.30 bits, which is well-separated from the null hypothesis cost of 269.79 bits. Thus, the probability that the cost difference between any of these hypotheses and the null hypothesis will be greater than 60 is small. The cost range between these hypotheses and the null hypothesis were 139.79 and 99.08 bits, respectively. The cost range between the first hypothesis and the tenth hypothesis was



**Figure 5.** Illustrations of 2D and 3D structural interactions of mushroom tyrosinase, and mapping of compound 1 and arbutin onto Hypo 1. (A) Mapping of the docking conformation of compound 1 onto Hypo 1 in the active site of mushroom tyrosinase. (B) Hypo 1 agrees with the docking conformation of arbutin in the active site of mushroom tyrosinase. (C) Two-dimensional (2D) schematic representation of the interactions between compound 1 and active site residues of mushroom tyrosinase. (D) Two-dimensional (2D) schematic representation of the interactions between arbutin and active site residues of mushroom tyrosinase. (E) Pharmacophore model features of Hypo 1 with the docking conformation of compound 1 mapping onto the mushroom tyrosinase surface. (In 2D schemes, green dashed line denotes hydrogen-bond interaction; circles in distinct colors represent the relative hydrophobic and/or  $\pi-\pi$  interactions among compounds and active site residues.)

40.82 bits. Thus, we could expect the possibility of representing a true correlation in the data to be at least 75%–90%.

The top-ranked pharmacophore model, Hypo 1, exhibited the optimal predictive power and statistical significance, which were indicated by a high correlation coefficient ( $r = 0.9$ ), a low RMS deviation (1.44), and a cost deviation of 139.79. The RMS deviation of Hypo 1 (1.44) demonstrated the favorable predictive capability of Hypo 1. For a constructed model to be reliable, the lowest total cost should be far from the null cost. Accordingly, a null cost of 296.79 indicates that Hypo 1 shows the most favorable predictive capability. Hypo 1 consists of one hydrogen-bond donor, one hydrogen-bond acceptor, and two hydrophobic groups, as shown in Figure 4A. The most active compound, Compound 1 (Chlorophorin;  $IC_{50} = 0.26 \mu\text{M}$ , see Table 1), maps perfectly well to all features of Hypo 1 (see Figures 5A and 5C). Hypo 1 was subjected to further evaluation for determining its predictive capability.

**4. Pharmacophore Model Validation.** To validate the capability of Hypo 1 to correctly predict activities, we used it to

predict the activities of all the training set compounds. All compounds in the training set and test set were classified into three scales—highly active ( $<5 \mu\text{M}$ , denoted by +++), moderately active ( $5\text{--}100 \mu\text{M}$ , denoted by ++), and inactive ( $>100 \mu\text{M}$ , denoted by +). Table 1 shows the actual and estimated activity and references of the 30 compounds in the training set. The difference between actual and estimated activity values is represented as an error (ratio between the experimental and estimated activities), and it is assigned a negative symbol if the actual activity is higher than the estimated one. It was observed that the error values of all compounds were  $<10$ , which implied a difference of less than 1 order of magnitude between the estimated and actual activities. Of the 30 compounds, three highly active compounds were predicted to be moderately active, and one moderately active was predicted to be inactive. Thus, Hypo 1 could estimate the activity of the training set molecules with a small error.

The purpose of the pharmacophore hypothesis generation was not only to predict the activity of the training set

**Table 2.** Actual and Estimated IC<sub>50</sub> Values for the Test Set Based on the Best Pharmacophore Hypothesis Hypo 1

No.	name or code	estimated IC <sub>50</sub> <sup>a</sup> ( $\mu\text{M}$ )	actual IC <sub>50</sub> <sup>a</sup> ( $\mu\text{M}$ )	error	estimated scale	actual scale	ref
31	Cpd4	1.46	0.77	+1.89	+++	+++	26
32	Cpd39	1.02	1.63	-1.59	+++	+++	24
33	artocarbene	3.18	2.45	+1.29	+++	+++	24
34	DC17	2.49	3.68	-1.47	+++	+++	29
35	Monophenolase	1.51	4.7	-3.11	+++	+++	30
36	DC05	10.88	6.52	+1.66	+++	+++	29
37	TK14	8.61	9.06	-1.05	+++	+++	31
38	DC01	4.70	9.1	-1.93	+++	+++	29
39	TK5	3.59	11.77	-3.27	+++	+++	31
40	Cpd4	15.97	15.69	+1.01	++	++	32
41	2,3-trans-dihydromorin	11.09	21.1	-1.90	++	++	33
42	genistein	24.44	33	-1.35	++	++	34
43	Cpd12a	33.33	36.5	-1.09	++	++	35
44	Sideroxylon inerme	20.06	63	-3.14	++	++	36
45	Cpd25	91.06	80	+1.13	++	++	27
46	Cpd2b	106.99	170	-1.58	+	+	28
47	Daedalin A	70.44	194	-2.75	++	+	38
48	dioxinodehydroeckol	119.92	222.94	-1.85	+	+	37
49	Cpd2e	106.98	280	-2.61	+	+	39
50	Cpd10	107.19	302	-2.81	+	+	40

<sup>a</sup>Activity scale: highly active (<15  $\mu\text{M}$ , +++), moderately active (15–100  $\mu\text{M}$ , ++), and inactive (>100  $\mu\text{M}$ , +).

compounds but also to verify whether the pharmacophore model was capable of predicting the activity of compounds that were not included in the training set. To further verify the predictive capability of Hypo 1 for compounds that were structurally distinct from those included in the training set, a test set of 20 molecules was subjected to Hypo 1 pharmacophore mapping analysis. A correlation coefficient value of 0.85 was obtained between the estimated and actual values (see Table 2). All the test set molecules were predicted correctly, except for one inactive compound that was overestimated as being moderately active. To further evaluate the statistical relevance of the pharmacophore model, the Fischer validation method<sup>41</sup> was used to estimate the correlation between the chemical structures and their biological activity. The experimental activities for the training set were scrambled randomly by using the CatScramble program<sup>42</sup> in Discovery Studio 3.5, and the rearranged training set was then fed into HypoGen running. The 95% confidence level was selected by performing a cross-validation test, and 19 spreadsheets constructed by the CatScramble program were used to generate a hypothesis by using the same features as those used in generating the initial hypothesis (see Table S1 in the Supporting Information). None of the outcome hypotheses had a cost score lower than that of Hypo 1, which confirms that Hypo 1 was not obtained by chance.

**5. Pharmacophore-Based Screening of Small Molecules Obtained from Natural Products.** Hypo 1 was used to screen and identify the top 500 small molecules obtained from molecular docking. The top 10 candidates, A1–A10, were selected for conducting a tyrosinase inhibition test. The test result showed that the natural product A5 (IBS ID: STOCK1N-41085; see Figure S2 in the Supporting Information) substantially reduced tyrosinase activity to an extent greater than that reached if arbutin were used. To obtain molecules with similar or stronger inhibitory potency against tyrosinase, the chemical structure of A5 was used as a query to search the natural product databases. Natural products B1–B35 were selected and subjected to the tyrosinase inhibition

test (see the section titled “In Vitro Study”). Three compounds showed stronger inhibition activity than did arbutin, and one of them, B16, had the chemical structure of KFY (Figure S3 in the Supporting Information) exhibiting appropriate complementarities with the pharmacophore model, Hypo1 (Figure S4 in the Supporting Information).

**In Vitro Study.** *1. Tyrosinase Inhibition Test.* Natural products A1–A10, which were selected from the top 500 docking results and simultaneously assessed by using Hypo 1, were investigated for their inhibitory activity against tyrosinase. The A5 molecule exhibits inhibitory activity that is superior to the inhibitory activity of  $\beta$ -arbutin (see Figure S2 in the Supporting Information). Natural products B1–B35, which were selected because of structural features similar to those of A5, were subsequently investigated for their inhibitory activity against mushroom tyrosinase. The tyrosinase inhibition test demonstrated that natural products B16 (IBS ID: STOCK1N-51005), B22 (IBS ID: STOCK1N-58256), B25 (IBS ID: STOCK1N-66238), and B26 (IBS ID: STOCK1N-66592) showed higher inhibitory activity, compared with the others (see Figure S3 in the Supporting Information). To further compare their inhibitory potency with arbutin and the A5 molecule, an inhibitory assay was performed in the presence of these compounds at 0.4 and 0.8 mM. The assay results showed that the B16 molecule exhibited superior inhibitory activity compared with arbutin (B16  $\geq$  A5 > arbutin), and notably, the chemical structure of B16 was determined to be equivalent to that of KFY (see Figure S4 in the Supporting Information).

Considering that B16 has the chemical structure of KFY, we attempted to synthesize a set of tripeptides with residues properties similar to those of KFY and evaluated their inhibitory activity against tyrosinase. Eleven (11) KFY-derived tripeptides were synthesized: FFY, KDY, KKY, KNY, KVY, NFY, RCY, RWY, VFY, DFY, and CRY (see Figure S5 in the Supporting Information). The inhibitory assay result demonstrated that eight tripeptides, including KFY, exhibited inhibitory activity greater than that of arbutin (see Figure 6, as well as Table S3 in the Supporting Information), and the

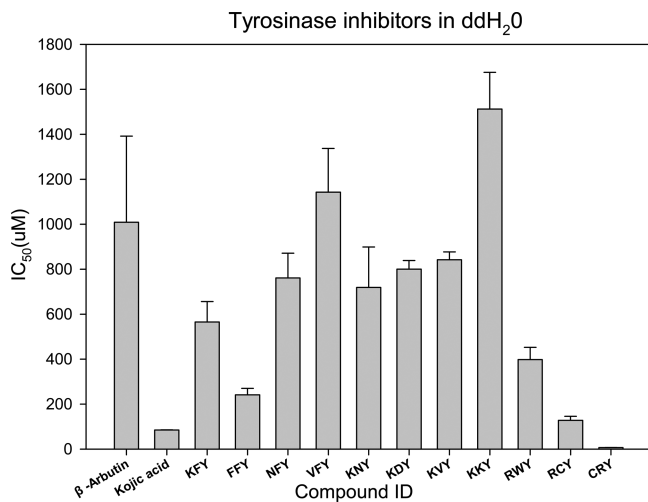


Figure 6. Mushroom tyrosinase inhibition activity test for tripeptides.

IC<sub>50</sub> values of CRY, RCY, FFY, and RWY were all below 0.5 mM. In particular, CRY showed the strongest inhibition activity, which was even stronger than that of kojic acid. Under doubly distilled water (ddH<sub>2</sub>O), the IC<sub>50</sub> value of CRY was 6.16 μM, which was far below the IC<sub>50</sub> value of arbutin, 1008.7 μM (see Table S3 in the Supporting Information).

## ■ DISCUSSION

In this study, by using ligand-based pharmacophore modeling, we systematically investigated the quantitative structure–activity relationship of tyrosinase and its inhibitors. Hypo 1 was the optimal pharmacophore hypothesis, characterized by the highest cost difference (139.79), lowest RMS deviation (1.44), and highest correlation coefficient ( $r = 0.9$ ). The difference between the total and fixed costs for Hypo 1 was 31.99 bits, which was the smallest among all differences, indicating a high probability of the true correlation of the data. Thus, Hypo 1 was statistically the most relevant model. The validation of Hypo demonstrated that it could accurately estimate the activities of training set and test set compounds with the smallest errors. The correlation coefficients for the estimated versus actual values for the training set and test set were 0.91 and 0.85, respectively, indicating high correlation between estimated and actual activities (see Figure S6 in the Supporting Information). Furthermore, the high correlation indicates the favorable predictive capability of Hypo 1. It is clear from the results of the cross-validation that all trials showed a correlation value of  $r < 0.9$  (see Table S1 in the Supporting Information), and the total cost and RMS deviation were higher than those of Hypo 1, indicating that none of the pharmacophore models showed a stronger predictive capability after randomization compared with Hypo 1. Therefore, the cross-validation results confirmed the accuracy and reliability of Hypo 1 with statistical significance.

As the most active compound in the training set, compound 1 showed a favorable fit with all the features of Hypo 1. The hydrogen-bond donor feature was occupied by the hydroxyl group of 2,4-dihydroxystyryl in compound 1. The hydrogen-bond acceptor feature was mapped onto one of the two symmetrical hydroxyl groups of benzene-1,3-diol. In addition, compound 1 matched the two hydrophobic features at the benzene ring of 2,4-dihydroxystyryl and the carbon tail of 3,7-dimethylocta-2,6-diene (Figure 5A). The 3D models of Hypo 1

and the corresponding small molecules (compound 1 and arbutin) in the active site of mushroom tyrosinase were determined through molecular docking. As shown in Figures 5C and 5E, we found that the hydroxyl group of 2,4-dihydroxystyryl in compound 1 functioned as a hydrogen-bond donor to interact with the Glu256 residue; the hydroxyl group of benzene-1,3-diol served as a hydrogen-bond acceptor to interact with the Asn260 residue. Moreover, the indole ring of Trp227 and the side chain of Met257 interacted with the hydrophobic carbon tail of 3,7-dimethylocta-2,6-diene. The side chains of Phe264 and Val283 interacted with the benzene rings of benzene-1,3-diol and 2,4-dihydroxystyryl via hydrophobic interactions, respectively. The pharmacophore model mapping also revealed that arbutin may interact with tyrosinase by employing similar chemical complementarities (see Figures 5B and 5D); however, additional hydrophobic interactions with the residues of Met257 and Trp227 were absent. These results indicated that Hypo 1 is reasonable and reliable for small molecule screening.

The use of GOLD molecular docking analysis, together with Hypo 1 pharmacophore screening, pruned the 47 263 natural resources to 10 natural products (A1–A10). The tyrosinase inhibition test showed that A5 effectively inhibits tyrosinase (see Figure S2 in the Supporting Information). The chemical structure of the A5 molecule shows two major moieties: Core1 and Core2 (recall Figure 4B). Core1 is similar to tyrosine, and Core2 is similar to a coumarin derivative. Tyrosine is the cognate substrate of tyrosinase, which suggests that the A5 molecule may adopt a tyrosine-like binding mode to interact with tyrosinase. The Hypo 1 pharmacophore mapping showed that Core1 is mapped with the hydrogen-bond donor and one hydrophobic feature, whereas Core2 is mapped with the hydrogen-bond acceptor and one hydrophobic feature. This result indicated that our approach combining molecular docking and pharmacophore screening successfully revealed the possibly crucial complementary functional group that plays an important part in tyrosinase inhibition, and points to the highly predictive capability of Hypo 1.

Natural compound B16 has the chemical structure of KFY, which shows proper complementarities with Hypo 1 model (see Figure S4 in the Supporting Information) and exhibits potent tyrosinase inhibitory activity (IC<sub>50</sub> = 564.9 μM). Furthermore, the structure of A5 is also similar to that of the dipeptide WY. Accordingly, the tyrosine residue at the C-terminus has a tendency to substantially contribute to the tyrosinase inhibitory activity of dipeptide-like compounds (A5) and tripeptides (KFY). By considering the tyrosine residue constraint and the biochemical and biophysical properties of K (lysine) and F (phenylalanine), a set of tripeptides were synthesized and investigated for their tyrosinase inhibitory activity. The tripeptides KNY, NFY, KDY, KVY, KKY, and VFY were less effective than was KFY (see Figure 6, as well as Table S3 in the Supporting Information), indicating that the inhibitory activity decreases when the residues at the middle of the tripeptides are substituted with N (Asp), D (Glu), and V (Val) residues. This finding is in agreement with a report which stated that peptides containing aspartic or glutamic acid residues usually do not bind very well to tyrosinase and the negative charge is not favorable for tyrosinase binding.<sup>14</sup> By contrast, four tripeptides showed considerably inhibitory potency, and their hierarchy of IC<sub>50</sub> was in the order CRY > RCY > FFY > RWY > KFY (see Figure 6, as well as Table S3 in the Supporting Information). This observation revealed that the replacement of residues at

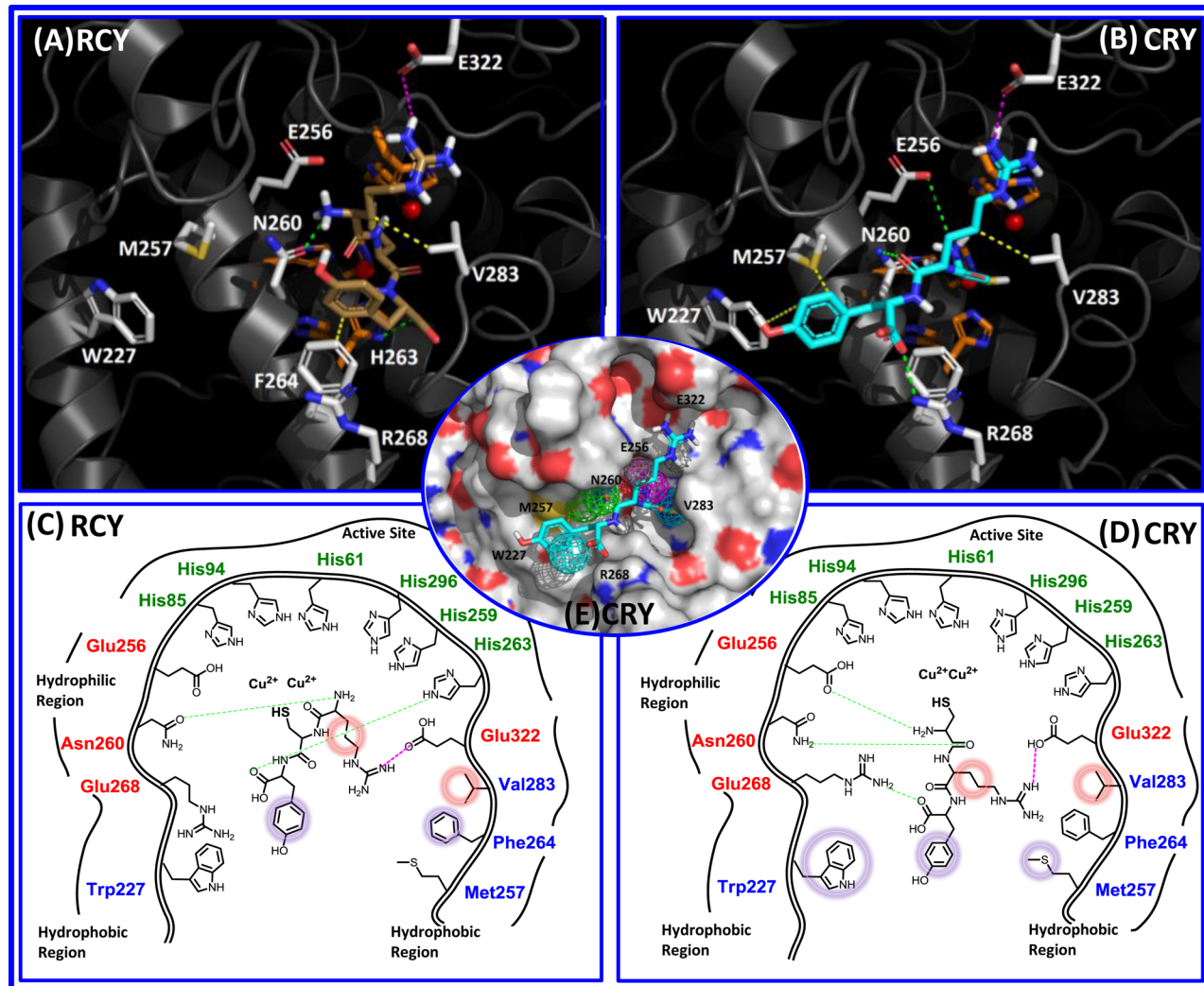


**Figure 7.** Illustrations of 2D and 3D structural interactions between mushroom tyrosinase and CRY and RCY mapping onto Hypo 1. (A) The docking conformation of RCY in the active site of mushroom tyrosinase. (B) The docking conformation of CRY in the active site of mushroom tyrosinase. (C) Two-dimensional (2D) schematic representation of pharmacophore mapping and interactions among RCY and active site residues of mushroom tyrosinase. (D) Two-dimensional (2D) schematic representation of pharmacophore mapping together with interactions between arbutin and active site residues of mushroom tyrosinase. (E) Pharmacophore model features of Hypo 1 with the docking conformation of tripeptide CRY mapping onto the mushroom tyrosinase surface. (In the 2D schemes, the green dashed line denotes hydrogen-bond interaction; circles in distinct colors represent the relative hydrophobic and/or  $\pi-\pi$  interactions among compounds and active site residues.)

the N-terminus and/or the middle position of tripeptides with R (Arg), C (Cys), and F (Phe) considerably increases tyrosinase inhibitory potency. This finding is consistent with previous reports, according to which Arg residue is essential and specific for tyrosine-peptide interaction.<sup>14,21</sup> The importance of Phe results from Phe being structurally similar to tyrosine, which is the natural substrate of tyrosinase;<sup>14</sup> peptides containing the polar, uncharged residue Cys are also good tyrosinase inhibitors.<sup>14,21</sup> The pharmacokinetic profile of all the tripeptides under investigation (except for the tripeptide DFY, which is insoluble in doubly distilled water (ddH<sub>2</sub>O)) was predicted by means of five precalculated ADMET (Absorption, Distribution, Metabolism, Excretion, and Toxicity) models provided by the Discovery Studio 3.5. (See Table S3 in the Supporting Information.) The results show that all of the tripeptides are within the high-to-low oral intestinal absorption level, low-to-undefined level of blood-brain penetration, and without hepatotoxicity. In addition, these tripeptides are

predicted to be false in cytochrome P450 2D6 enzyme inhibition and binding with carrier proteins in the blood.

CRY particularly showed the most striking tyrosinase inhibitory activity, with a lower IC<sub>50</sub> value (6.16  $\mu$ M) compared to kojic acid (IC<sub>50</sub> = 84.4  $\mu$ M, in ddH<sub>2</sub>O) and arbutin (IC<sub>50</sub> = 1008.7  $\mu$ M, in ddH<sub>2</sub>O). By contrast, RCY, with the reversed arrangement of the R/C residues of CRY, exhibited an IC<sub>50</sub> value that was only 1/21 of that of CRY. The comparisons of the molecular dynamics (MD) simulation show that tripeptide CRY has a RMS deviation of <0.9  $\text{\AA}$  and the tyrosinase structure has a RMS deviation of ~1.32  $\text{\AA}$ , indicating that docking has a comparable result to MD (see Figure S7 in the Supporting Information). Therefore, our molecular docking of tripeptides was reliable. The pharmacophore model mapping and molecular docking analyses revealed that CRY fitted well with all the features of Hypo 1 and was complementary to the active site residues of tyrosinase (see Figure 7E). As shown in Figures 7B and 7D, Arg of CRY possibly showed electrostatic and hydrophobic interactions with Glu322 and Val283 residues,

respectively, in the active site of mushroom tyrosinase. The Tyr residue of CRY interacted with the side chains of Trp227 and Met257 of tyrosinase through hydrophobic interactions. In addition, three hydrogen-bond interactions were observed between CRY and tyrosinase. However, tripeptide RCY neither fitted well with all of the features of Hypo 1 nor interacted with as many residues as CYR did in the active site of mushroom tyrosinase (see Figures 7A and 7C), accounting for the difference in the tyrosinase inhibitory potency between CRY and RCY. Therefore, we propose that cysteine residue, predominant at the C-terminus of the tripeptide, contributes significantly to tyrosinase inhibition. Moreover, the thiol-containing amino acid cysteine has been reported as a strong tyrosinase inhibitor.<sup>8,43,44</sup> The coordination of the sulfur atom of PTU (phenylthiourea) with the dicopper active site inhibits tyrosinase-like catechol oxidase.<sup>45</sup> It has also been proposed that tyrosinase can be inhibited by promoting its interaction with cysteine via chelation of Cu ions.<sup>46</sup> Since both the thiol groups of cysteine residues of CRY and RCY were close to the Cu ions in the active site of mushroom tyrosinase (see Figures 7C and 7D), we suggest that CRY and RCY may use the S atom of the thiol group in the cysteine moiety to coordinate with Cu ions in the active site of tyrosinase and function as a Cu chelator.

Tyrosinase inhibitory peptides such as dipeptides,<sup>20</sup> cyclic peptides,<sup>23</sup> short-sequence oligopeptides,<sup>21</sup> and kojic acid–tripeptide compounds<sup>22</sup> have been investigated. Our designed tripeptide CRY shows greater tyrosinase inhibitory potency, compared to short-sequence oligopeptides—the IC<sub>50</sub> value of CRY (6.16 μM) is much lower than those of the oligopeptides<sup>21</sup> (40 μM to 8 mM). In addition, the mushroom tyrosinase inhibitory activity of CRY is as good as that of the kojic acid–tripeptide compounds<sup>22</sup> (Ko-FWW, IC<sub>50</sub> = 6.17 μM). Among the dipeptides that show a wide variation in their inhibition effect on mushroom polyphenol oxidase (PPO) activity and dipeptides,<sup>20</sup> GD, GG, GY, GF, and GK prevent melanin formation by directly inhibiting the enzyme-catalyzed reaction. Given that the chemical structure of the A5 molecule resembles that of WY, dipeptides derived from WY have high potential for use in tyrosinase inhibitor development.

## CONCLUSION

In this study, structure-based molecular docking and ligand-based pharmacophore modeling methods were combined to construct a reasonable and reliable pharmacophore model (Hypo 1) to identify crucial complementary functional groups, which are essential for mushroom tyrosinase inhibition. It was observed that natural compound A5 resembles the chemical structure of the dipeptide (WY) and that B16 has the structure of a tripeptide (KFY), revealing that the C-terminus tyrosine residue plays an important role in mushroom tyrosinase inhibition. RCY and CRY showed high tyrosinase inhibitory potency among other tripeptides, indicating that the positional and functional preference of the cysteine residue at the N-terminus of the tripeptides mainly determines the tyrosinase inhibition activity. CRY and RCY use the thiol group of the cysteine residue to coordinate with the Cu ions in the active site of tyrosinase, thereby showing low tyrosinase activity. We discovered a novel tripeptide, CRY, with the most striking inhibitory potency against mushroom tyrosinase (IC<sub>50</sub> = 6.16 μM); it is more desirable than the known oligopeptides, and it is comparable with the kojic acid–tripeptide compound. These results provide an insight into the structural and functional

roles of key amino acids in CRY, which was derived from a natural compound. The results of this study are expected to be useful for the development of tyrosinase inhibitors.

## MATERIALS AND METHODS

**Materials.** Molecular docking studies were conducted using Genetic Optimization for Ligand Docking (GOLD; GlaxoSmithKline PLC, Astex Technology, Ltd., CCDC). The generation of all pharmacophore models and Hypo 1-based virtual screening were performed using HypoGen implemented in Discovery Studio 3.5. All the calculations were performed at the National Center for High-Performance Computing, Taiwan. Mushroom tyrosinase, L-tyrosine, and potassium phosphate buffer (PBS) (67 mM, pH 6.8) were purchased from Sigma-Aldrich (St. Louis, MO). Natural products were obtained from four companies: InterBioScreen (IBS), Specs, Novartis Consumer Health, and NATx. All peptides used in this study were custom-synthesized by Kelowna International Scientific, Inc. (New Taipei, Taiwan) with a purity of >95%.

**Methods.** *1. Molecular Docking and Molecular Dynamics Simulation.* The Sketch Molecules and Prepare Ligands modules implemented in Discovery Studio 3.5 (Accelrys Software, Inc., San Diego, CA, USA) were used to create the molecular structures of all compounds, and hydrogen atoms were present in all the constructed ligands. Then, energy was minimized to optimize compound conformations. Furthermore, the GOLD docking program (Cambridge Crystallographic Data Center (CCDC), version 5.1) with the GoldScore scoring function was employed for molecular docking analysis. The constructed and energy-minimized compounds were subsequently docked into the active site of mushroom tyrosinase with modified docking parameter settings (number of operations and population size values were 1 600 000 and 1000, respectively; default settings were used for the other parameters). The most possible orientations and positions with the most favorable free energy were examined and presented.

The tyrosinase-CRY complex model was simulated with the AMBER package using the AMBER FF99 all-hydrogen amino acid parameters. From docking simulations, the complex structure was generated and then inserted into the TIP3P water box. All MD simulations were performed in the canonical ensemble with a simulation temperature of 310 K, unless stated otherwise, by using the Verlet integrator with an integration time step of 0.002 ps and SHAKE constraints<sup>47</sup> of all covalent bonds involving H atoms. In the electrostatic interactions, atom-based truncation was performed using the PME<sup>48</sup> method, and the switch van der Waals function was used with a 2.00 nm cutoff for atom-pair lists. The complex structure was minimized for 100 000 conjugate gradient steps, and was then subjected to a 20 000 ps isothermal, constant volume MD simulation. Over the 1000 ns MD trajectories of the tripeptide CRY with solvent molecules and tyrosinase, the overall structure of complexes appeared to be equilibrated after 21 ps. Here, we show the potential energy and RMS deviation of the complex system of tripeptide CRY with the MD simulation (see Figure S7 in the Supporting Information). Finally, various interactions involved in the protein/ligand complex were analyzed using Ligplot 4.0.<sup>49,50</sup> The molecular visualization and the construction of the electronic potential surface map of the complex were achieved by using PyMOL software (<http://www.pymol.org>).

*2. Pharmacophore Modeling.* The training set, which consisted of 30 compounds,<sup>24–28</sup> was selected by considering

the structural diversity and the wide variety of activity ranges presented in Figure 2. Inhibitory activities against tyrosinase in the training set were reported as  $IC_{50}$  values ranging from 0.26  $\mu\text{M}$  to 346  $\mu\text{M}$ , covering 4 orders of magnitude (recall Table 1). All structures were built and minimized to the closest local minimum by using a modified CHARMM force field<sup>51</sup> in the Catalyst program implemented in Discovery Studio 3.5 (Accelrys Software, Inc., San Diego, CA, USA), and the CAESAR algorithm<sup>52</sup> was used for conformational analysis of each molecule. In this study, the maximum value of the setting number of the conformer was limited to 250 by using the “best conformers generation” method with a 20 kcal/mol energy cutoff, and the default setting was used for the rest of the parameters. Four features—hydrogen-bond acceptor, hydrogen-bond donor, excluded volumes, and hydrophobic features—were selected to generate the pharmacophore hypothesis; the 3D QSAR Pharmacophore Generation (HypoGen) module in Discovery Studio 3.5 was used. In addition, the HypoGen program with the default uncertainty value of 2 for each compound was used to find pharmacophore models that contain a maximum of four features.

**3. Inhibition Assay.** Natural products (**A1–A10** and **B1–B35**) and tripeptides (FFY, KDY, KKY, KNY, KVY, NFY, RCY, RWY, VFY, DFY, and CRY) were dissolved in doubly distilled water (ddH<sub>2</sub>O) to prepare inhibitor solutions with different concentrations. Tyrosinase inhibitory activity was determined *in vitro*, using L-tyrosine as the substrate and according to the method of Piao et al.<sup>53</sup> The experiment was conducted in a 96-well flat-bottom plate. First, 80  $\mu\text{L}$  of 67 mM potassium phosphate buffer (NaH<sub>2</sub>PO<sub>4</sub>–Na<sub>2</sub>HPO<sub>4</sub>, pH 6.8), 25  $\mu\text{L}$  of 5 mM inhibitor solution, and 125  $\mu\text{L}$  of 5 mM L-tyrosine were added into each well and incubated at 25 °C for 5 min. Then, 20  $\mu\text{L}$  of 1250 U/mL mushroom tyrosinase solution was then added to each well to obtain a final volume of 250  $\mu\text{L}$  and the mixtures were incubated at 25 °C for another 5 min. Subsequently, the amount of dopachrome produced in the reaction solution was determined against a blank solution without tyrosinase by using a spectrophotometer (Varian Cary, Model 50 Bio UV-visible spectrophotometer) at 475 nm for 10 min. We recorded the dopachrome accumulation every 10 s for 10 min and determined the inhibition at 0.4 and 0.8 mM for all compounds and tripeptides. In addition, arbutin and kojic acid, which were used as the positive control inhibitors, were tested at the same concentrations and conditions.

**4.  $IC_{50}$  Determination.** The  $IC_{50}$  value (denoting the concentration of a compound that causes 50% inhibition) of arbutin, kojic acid, and all tripeptides was determined. Inhibitory activity was expressed as the concentration that inhibited 50% of tyrosinase activity, and it was designated as  $IC_{50}$ . In the process of determining  $IC_{50}$ , arbutin and kojic acid were used as positive control inhibitors. Technically and experimentally, the  $IC_{50}$  value is generally obtained by considering the X-axis on an inhibitor concentration versus product formation curve and the alignment of the dose response curve, relative to the dependent Y-axis. In the present study, dose-dependent inhibition experiments were performed in triplicate to determine the  $IC_{50}$  values of the test compounds. From the average percentage inhibition for the three doses, log-linear curves and their equations were determined. To ensure the reproducibility of the results, all studies were performed at least in triplicate and the mean values were reported.

**5. Statistical Analysis.** The reaction correlated with the amount of dopachrome produced was determined according to a previously described method.<sup>54</sup> The tyrosinase activity was calculated using the following equation:

$$\text{tyrosinase activity (\%)} = \left[ \frac{S - B}{C} \right] \times 100$$

where S is the OD<sub>475</sub> absorbance of the test compound, B is the OD<sub>475</sub> absorbance of the blank, and C is the OD<sub>475</sub> absorbance of the control.

## ■ ASSOCIATED CONTENT

### ■ Supporting Information

Seven figures (Figures S1, S2, S3, S4, S5, S6, and S7), three tables (Tables S1, S2, and S3), and supplemental references are available as Supporting Information. This material is available free of charge via the Internet at <http://pubs.acs.org>.

## ■ AUTHOR INFORMATION

### Corresponding Author

\*Address: National Research Institute of Chinese Medicine, No. 155-1, Sec. 2, Linong St., Beitou District, Taipei 11221, Taiwan. Tel.: (886)-2-2820-1999, ext. 6241. Fax: (886)-2-2823-6367. E-mail: tkc@nricm.edu.tw.

### Notes

The authors declare no competing financial interest.

## ■ ACKNOWLEDGMENTS

We thank Chia-Ying Wu (Institute of Biotechnology, National Changhua University of Education, Changhua, Taiwan), Jin-Yu Shiu (Institute of Biotechnology, National Changhua University of Education, Changhua, Taiwan), and Chia-Chia Chang (Institute of Biotechnology, National Changhua University of Education, Changhua, Taiwan) for fruitful discussions and their help. We are grateful to the National Center for High-Performance Computing for computer time and facilities. The computational work using GOLD, AMBER and Discovery Studio were conducted at the National Center for High-Performance Computing, Taiwan. This work was supported by the National Research Institute of Chinese Medicine (No. 103T51-11) and the National Science Council, Taipei, Taiwan (Nos. NSC 100-2320-B-077-004-MY2 and NSC 103-2320-B-077-001-MY3, awarded to K.-C.T.).

## ■ REFERENCES

- (1) Costin, G. E.; Hearing, V. J. Human skin pigmentation: Melanocytes modulate skin color in response to stress. *FASEB J.* **2007**, *21*, 976–994.
- (2) Alexis, A.; Barbosa, V. H., Eds. *Skin of Color: A Practical Guide to Dermatologic Diagnosis and Treatment*; Springer: Berlin, Heidelberg, 2013.
- (3) Piampongsant, T. Treatment of melasma: A review with personal experience. *Int. J. Dermatol.* **1998**, *37*, 897–903.
- (4) Cavalieri, E. L.; Li, K. M.; Balu, N.; Saeed, M.; Devanesan, P.; Higginbotham, S.; Zhao, J.; Gross, M. L.; Rogan, E. G. Catechol ortho-quinones: The electrophilic compounds that form depurinating DNA adducts and could initiate cancer and other diseases. *Carcinogenesis* **2002**, *23*, 1071–1077.
- (5) Kim, Y. J.; Uyama, H. Tyrosinase inhibitors from natural and synthetic sources: Structure, inhibition mechanism and perspective for the future. *Cell. Mol. Life Sci.* **2005**, *62*, 1707–1723.
- (6) Eisenhofer, G.; Tian, H.; Holmes, C.; Matsunaga, J.; Roffler-Tarlov, S.; Hearing, V. J. Tyrosinase: A developmentally specific major determinant of peripheral dopamine. *FASEB J.* **2003**, *17*, 1248–1255.

- (7) Chang, T. S. An updated review of tyrosinase inhibitors. *Int. J. Mol. Sci.* **2009**, *10*, 2440–2475.
- (8) Slominski, A.; Tobin, D. J.; Shibahara, S.; Wortsman, J. Melanin pigmentation in mammalian skin and its hormonal regulation. *Physiol. Rev.* **2004**, *84*, 1155–1228.
- (9) Pan, T.; Li, X.; Jankovic, J. The association between Parkinson's disease and melanoma. *Int. J. Cancer* **2011**, *128*, 2251–2260.
- (10) Asanuma, M.; Miyazaki, I.; Ogawa, N. Dopamine- or L-DOPA-induced neurotoxicity: The role of dopamine quinone formation and tyrosinase in a model of Parkinson's disease. *Neurotox Res.* **2003**, *5*, 165–176.
- (11) Seo, S. Y.; Sharma, V. K.; Sharma, N. Mushroom tyrosinase: Recent prospects. *J. Agric. Food Chem.* **2003**, *51*, 2837–2853.
- (12) Elsner, P.; Maibach, H. I. *Cosmeceuticals: Drugs vs. Cosmetics; Cosmetic Science and Technology Series, Vol. 23*; Marcel Dekker: New York, 2000.
- (13) Maeda, K.; Fukuda, M. Arbutin: Mechanism of its depigmenting action in human melanocyte culture. *J. Pharmacol. Exp. Ther.* **1996**, *276*, 765–769.
- (14) Schurink, M.; van Berkel, W. J.; Wichters, H. J.; Boeriu, C. G. Novel peptides with tyrosinase inhibitory activity. *Peptides* **2007**, *28*, 485–495.
- (15) Germanas, J. P.; Wang, S.; Miner, A.; Hao, W.; Ready, J. M. Discovery of small-molecule inhibitors of tyrosinase. *Bioorg. Med. Chem. Lett.* **2007**, *17*, 6871–6875.
- (16) Smith, M. T.; Yager, J. W.; Steinmetz, K. L.; Eastmond, D. A. Peroxidase-dependent metabolism of benzene's phenolic metabolites and its potential role in benzene toxicity and carcinogenicity. *Environ. Health Perspect.* **1989**, *82*, 23–29.
- (17) Rossi, L.; Moore, G. A.; Orrenius, S.; O'Brien, P. J. Quinone toxicity in hepatocytes without oxidative stress. *Arch. Biochem. Biophys.* **1986**, *251*, 25–35.
- (18) DeCaprio, A. P. The toxicology of hydroquinone—Relevance to occupational and environmental exposure. *Crit. Rev. Toxicol.* **1999**, *29*, 283–330.
- (19) Fuyuno, I. Spotlight turns on cosmetics for Asian skin. *Nature* **2004**, *432*, 938.
- (20) Girelli, A. M.; Mattei, E.; Messina, A.; Tarola, A. M. Inhibition of polyphenol oxidases activity by various dipeptides. *J. Agric. Food Chem.* **2004**, *52*, 2741–2745.
- (21) Abu Ubeid, A.; Zhao, L.; Wang, Y.; Hantash, B. M. Short-sequence oligopeptides with inhibitory activity against mushroom and human tyrosinase. *J. Invest. Dermatol.* **2009**, *129*, 2242–2249.
- (22) Kim, H.; Choi, J.; Cho, J. K.; Kim, S. Y.; Lee, Y. S. Solid-phase synthesis of kojic acid-tripeptides and their tyrosinase inhibitory activity, storage stability, and toxicity. *Bioorg. Med. Chem. Lett.* **2004**, *14*, 2843–2846.
- (23) Morita, H.; K, T.; Kobata, H.; Gonda, A.; Takeya, K.; Itokawa, H. Pseudostellarins D–F, new tyrosinase inhibitory cyclic peptides from *Pseudostellaria heterophylla*. *Tetrahedron* **1994**, *9975–9982*.
- (24) Shimizu, K.; Kondo, R.; Sakai, K. Inhibition of tyrosinase by flavonoids, stilbenes and related 4-substituted resorcinols: Structure–activity investigations. *Planta Med.* **2000**, *66*, 11–15.
- (25) Zheng, Z. P.; Cheng, K. W.; To, J. T.; Li, H.; Wang, M. Isolation of tyrosinase inhibitors from *Artocarpus heterophyllus* and use of its extract as antibrowning agent. *Mol. Nutr. Food Res.* **2008**, *52*, 1530–1538.
- (26) Tajima, R.; Oozeki, H.; Muraoka, S.; Tanaka, S.; Motegi, Y.; Nihei, H.; Yamada, Y.; Masuoka, N.; Nihei, K. Synthesis and evaluation of bibenzyl glycosides as potent tyrosinase inhibitors. *Eur. J. Med. Chem.* **2011**, *46*, 1374–1381.
- (27) Bao, K.; Dai, Y.; Zhu, Z. B.; Tu, F. J.; Zhang, W. G.; Yao, X. S. Design and synthesis of biphenyl derivatives as mushroom tyrosinase inhibitors. *Bioorg. Med. Chem.* **2010**, *18*, 6708–6714.
- (28) Yi, W.; Cao, R.; Peng, W.; Wen, H.; Yan, Q.; Zhou, B.; Ma, L.; Song, H. Synthesis and biological evaluation of novel 4-hydroxybenzaldehyde derivatives as tyrosinase inhibitors. *Eur. J. Med. Chem.* **2010**, *45*, 639–646.
- (29) Casanola-Martin, G. M.; Marrero-Ponce, Y.; Tareq Hassan Khan, M.; Torrens, F.; Perez-Gimenez, F.; Rescigno, A. Atom- and bond-based 2D TOMOCOMD-CARDD approach and ligand-based virtual screening for the drug discovery of new tyrosinase inhibitors. *J. Biomol. Screen.* **2008**, *13*, 1014–1024.
- (30) Ryu, Y. B.; Westwood, I. M.; Kang, N. S.; Kim, H. Y.; Kim, J. H.; Moon, Y. H.; Park, K. H. Kurarinol, tyrosinase inhibitor isolated from the root of *Sophora flavescens*. *Phytomedicine* **2008**, *15*, 612–618.
- (31) Marrero-Ponce, Y.; Khan, M. T.; Casanola-Martin, G. M.; Ather, A.; Sultankhozhzaev, M. N.; Garcia-Domenech, R.; Torrens, F.; Rotondo, R. Bond-based 2D TOMOCOMD-CARDD approach for drug discovery: Aiding decision-making in “in silico” selection of new lead tyrosinase inhibitors. *J. Comput. Aided Mol. Des.* **2007**, *21*, 167–188.
- (32) Ahmad, V. U.; Ullah, F.; Hussain, J.; Farooq, U.; Zubair, M.; Khan, M. T.; Choudhary, M. I. Tyrosinase inhibitors from *Rhododendron collettianum* and their structure–activity relationship (SAR) studies. *Chem. Pharm. Bull. (Tokyo)* **2004**, *52*, 1458–1461.
- (33) Zheng, Z. P.; Zhu, Q.; Fan, C. L.; Tan, H. Y.; Wang, M. Phenolic tyrosinase inhibitors from the stems of *Cudrania cochinchinensis*. *Food Funct.* **2011**, *2*, 259–264.
- (34) Kim, J. M.; Ko, R. K.; Jung, D. S.; Kim, S. S.; Lee, N. H. Tyrosinase inhibitory constituents from the stems of *Maackia fauriei*. *Phytother. Res.* **2010**, *24*, 70–75.
- (35) Yi, W.; Cao, R.; Wen, H.; Yan, Q.; Zhou, B.; Ma, L.; Song, H. Discovery of 4-functionalized phenyl-O-beta-D-glycosides as a new class of mushroom tyrosinase inhibitors. *Bioorg. Med. Chem. Lett.* **2009**, *19*, 6157–6160.
- (36) Momtaz, S.; Mapunya, B. M.; Houghton, P. J.; Edgerly, C.; Hussein, A.; Naidoo, S.; Lall, N. Tyrosinase inhibition by extracts and constituents of *Sideroxylon inerme* L. stem bark, used in South Africa for skin lightening. *J. Ethnopharmacol.* **2008**, *119*, 507–512.
- (37) Yoon, N. Y.; Eom, T. K.; Kim, M. M.; Kim, S. K. Inhibitory effect of phlorotannins isolated from *Ecklonia cava* on mushroom tyrosinase activity and melanin formation in mouse B16F10 melanoma cells. *J. Agric. Food Chem.* **2009**, *57*, 4124–4129.
- (38) Morimura, K.; Yamazaki, C.; Hattori, Y.; Makabe, H.; Kamo, T.; Hirota, M. A tyrosinase inhibitor, Daedalin A, from mycelial culture of *Daedalea dickinsii*. *Biosci., Biotechnol., Biochem.* **2007**, *71*, 2837–2840.
- (39) Yi, W.; Cao, R.; Wen, H.; Yan, Q.; Zhou, B.; Wan, Y.; Ma, L.; Song, H. Synthesis and biological evaluation of helcid analogues as mushroom tyrosinase inhibitors. *Bioorg. Med. Chem. Lett.* **2008**, *18*, 6490–6493.
- (40) Matos, M. J.; Santana, L.; Uriarte, E.; Delogu, G.; Corda, M.; Fadda, M. B.; Era, B.; Fais, A. New halogenated phenylcoumarins as tyrosinase inhibitors. *Bioorg. Med. Chem. Lett.* **2011**, *21*, 3342–3345.
- (41) John, S.; Thangapandian, S.; Sakkiah, S.; Lee, K. W. Potent BACE-1 inhibitor design using pharmacophore modeling, in silico screening and molecular docking studies. *BMC Bioinf.* **2011**, *12* (Suppl. 1), S28.
- (42) Sarma, R.; Sinha, S.; Ravikumar, M.; Kishore Kumar, M.; Mahmood, S. K. Pharmacophore modeling of diverse classes of p38 MAP kinase inhibitors. *Eur. J. Med. Chem.* **2008**, *43*, 2870–2876.
- (43) Tukamoto, T. T.; Taniguchi, T. Comparison of inhibitory effect of various chemical agents on tyrosinase activity by manometric method. *J. Invest. Dermatol.* **1958**, *30*, 305–310.
- (44) Jergil, B.; Lindbladh, C.; Rorsman, H.; Rosengren, E. Inactivation of human tyrosinase by cysteine. Protection by dopa and tyrosine. *Acta Derm. Venereol.* **1984**, *64*, 155–157.
- (45) Ghani, U.; Ullah, N. New potent inhibitors of tyrosinase: Novel clues to binding of 1,3,4-thiadiazole-2(3H)-thiones, 1,3,4-oxadiazole-2(3H)-thiones, 4-amino-1,2,4-triazole-5(4H)-thiones, and substituted hydrazides to the dicopper active site. *Bioorg. Med. Chem.* **2010**, *18*, 4042–4048.
- (46) Schurink, M. *Peptides as inhibitors of lipoxygenase and tyrosinase*. Thesis, Wageningen University, Wageningen, The Netherlands, 2007.
- (47) Ryckaert, J.-P.; Ciccotti, G.; Berendsen, H. J. C. Numerical integration of the cartesian equations of motion of a system with

constraints: Molecular dynamics of *n*-alkanes. *J. Comput. Phys.* **1977**, *23*, 327–341.

(48) Darden, T.; York, D.; Pedersen, L. Particle mesh Ewald: An *N*·log(*N*) method for Ewald sums in large systems. *J. Chem. Phys.* **1993**, *98*, 10089–10092.

(49) Laskowski, R. A.; Swindells, M. B. LigPlot+: Multiple ligand–protein interaction diagrams for drug discovery. *J. Chem. Inf. Model.* **2011**, *S1*, 2778–2786.

(50) Wallace, A. C.; Laskowski, R. A.; Thornton, J. M. LIGPLOT: A program to generate schematic diagrams of protein–ligand interactions. *Protein Eng.* **1995**, *8*, 127–134.

(51) Brooks, B. R.; Bruccoleri, R. E.; Olafson, B. D.; States, D. J.; Swaminathan, S.; Karplus, M. CHARMM: A program for macromolecular energy, minimization, and dynamics calculations. *J. Comput. Chem.* **1983**, *4*, 187–217.

(52) Li, J.; Ehlers, T.; Sutter, J.; Varma-O'Brien, S.; Kirchmair, J. CAESAR: A new conformer generation algorithm based on recursive buildup and local rotational symmetry consideration. *J. Chem. Inf. Model.* **2007**, *47*, 1923–1932.

(53) Piao, L. Z.; Park, H. R.; Park, Y. K.; Lee, S. K.; Park, J. H.; Park, M. K. Mushroom tyrosinase inhibition activity of some chromones. *Chem. Pharm. Bull. (Tokyo)* **2002**, *50*, 309–311.

(54) Takahashi, M.; Takara, K.; Toyozato, T.; Wada, K. A novel bioactive chalcone of *Morus australis* inhibits tyrosinase activity and melanin biosynthesis in B16 melanoma cells. *J. Oleo Sci.* **2012**, *61*, 585–592.